COMPARISON OF DOSE CALCULATION METHODS FOR A MANTLE FIELD IN THE RADIATION THERAPY OF HODGKIN'S DISEASE

A Thesis

Submitted to the Graduate Faculty of the
Louisiana State University and
Agricultural and Mechanical College
in partial fulfillment of the
requirements for the degree of
Master of Science
in
The Nuclear Science Center

by
Tracie D. Espenan
B.S., Louisiana Tech University, 1979
B.S., Northeast Louisiana University, 1981
August, 1986

Espenan, Tracie Davis, B.S. Louisiana Tech University, 1979
B.S. Northeast Louisiana University, 1981
Master of Science, Summer Commencement, 1986
Major: Nuclear Science
Comparison of Dose Calculation Methods for a Mantle Field in the Radiation Therapy of Hodgkin's Disease
Thesis directed by William S. Kubricht
Pages in Thesis,58. Words in Abstract, 169.

ABSTRACT

For most early cases of Hodgkin's disease, radiotherapy is the primary form of treatment and involves the use of large irregularly shaped fields for irradiation of affected lymph node chains. The dosimetry of irregularly-shaped fields is complex and must take into account the variations in radiation exposure across the entire treatment field. To prescribe an optimal course of radiotherapy for a patient with Hodgkin's disease, the radiotherapist must have accurate dosimetry. This study was undertaken to test the accuracy of the dosimetry of a mantle field for treatment of Hodgkin's disease patients at Mary Bird Perkins Cancer Treatment Center. A three-dimensional phantom, or model, of a human thorax was constructed and irradiated with the mantle treatment method. The phantom provided data to compare to doses calculated by three methods: Cundiff, et al. (1973) method, Perkins Cancer Center method, and Capintec Model RT110 computer method. It was found that the method of Cundiff, et al. (1973) was the most accurate for the dosimetry of the mantle field.

DEDICATION

to my Ma-ma

:o William

ımbremont,

for the

staff of

Treatment

eard and

or their

loving

ACKNOWLEDGEMENTS

The author would like to express her appreciation to William S. Kubricht, Jr., Dr. Sheldon A. Johnson, Dr. Edward N. Lambremont, and Dr. Ronald M. Knaus for their guidance and advice and for the opportunities for learning they provided.

Gratitude is also expressed to those members of the staff of both the Nuclear Science Center and Mary Bird Perkins Cancer Treatment Center who provided knowledge, help, and encouragement.

A special note of thanks is expressed to Mr. David Heard and St. Luke's, St. Margaret's, and Trinity Episcopal Churches for their contributions to this research.

This endeavor would not have been possible without the loving support and help of my husband, Greg.

TABLE OF CONTENTS

Page

DEDICATION ii

ACKNOWLEDGEMENTS iii

TABLE OF CONTENTS iv

LIST OF TABLES v

LIST OF FIGURES vi

ABSTRACT viii

CHAPTER ONE

Introduction
Background Information 1
Mantle Field Dosimetery 11

CHAPTER TWO

Materials and Methods 16

CHAPTER THREE

Results 23

CHAPTER FOUR

Discussion 30

REFERENCES 33

APPENDIX A

Data for Perkins Method of Calculation 37

APPENDIX B

Off-Axis Factors 42

APPENDIX C

Calculation of Scatter/Air Ratios 47

VITA 50

LIST OF TABLES

Table		Page
1.	Table of the measurement distances in cm used for dose calculation by the Perkins method. These distances were determined by measurement of the thoracic wax phantom	25
2.	The SAR for each point of calculation in the thoracic wax phantom as determined by the Capintec computer compared to the SAR for each point as determined by manual averaging, detailed by Cundiff, et al. (1973)	26
3.	Comparison of actual tissue dose (A) in cGy to the predictions of tissue dose in cGy by the Perkins method (B), the of Cundiff, et al. (1973) method (C), and the Capintec computer method	27
4.	Comparison of the predictions of tissue dose in cGy in patients by the Perkins method and the method of Cundiff, et al. (1973)	29
C.1.	An example of the calculation of the average scatter-air ratio to the point in Figure C.1	49

LIST OF FIGURES

Figure — Page

1. Incidence rates of Hodgkin's disease showing age in years versus incidence per million population. Adapted from Kaplan, (1972). 2

2. Diagram of the anatomic definition of separate lymph node regions. Taken from Kaplan (1972). 3

3. Diagramatic representation of the pathways of contiguous extension of Hodgkins disease from various hypothetical primary sites. Taken from Kaplan, 1972 5

4. Typical radiation field commonly employed in Hodgkin's disease. I = mantle field; II = para-aortic-splenic pedicle; III = pelvic. Taken from Rubin (1983). 9

5. Graph showing the results of different fractionation rates in humans versus total dose. Solid dots signify local tumor control; open dots signify failures. Taken from Fletcher (1980). 10

6. A diagram of the Lucite cube phantom used to ascertain the water-to-wax conversion factor. Adapted from Nelson (1985). 17

7. A. A sketch (not to scale) of the wax phantom, viewed from the abdomen to the chin. B. Side view of the wax phantom. Channels for the use of dosimeters are shown as follows: (a) Neck, (b) CAX, (c) Axilla, (d) Supraclavicular, (e) Mid-mediastinum, (f) Lower Mediastinum 19

A.1 Fractional depth dose for increasing field sizes and depths in cm for the Clinac 4 linear accelerator (Peterson and Golden, 1972) 38

A.2 Output correction factors for increasing field sizes in cm for a Clinac 4 linear accelerator at Perkins Cancer Center (Kubricht, 1986) 39

A.3 Field size dependence correction factors for a Clinac 4 linear accelerator at Perkins Cancer Center (Kubricht, 1986) 40

LIST OF FIGURES (Continued)

Figure Page

A.4 Backscatter correction factors for a Clinac 4 linear accelerator at Perkins Cancer Center (Kubricht, 1986) 41

B.1 Graph of the relationship between the off-axis factor and the distance in cm off the central axis, measured in water at a 13 mm depth (Kubricht, 1986) 43

B.2 Graph of the relationship between the off-axis factor and the distance in cm off the central axis, measured in water at a 5 cm depth (Kubricht, 1986) 44

B.3 Graph of the relationship between the off-axis factor and the distance in cm off the central axis, measured in water at a 10 cm depth (Kubricht, 1986) 45

B.4 Graphs showing the effects of increasing the field size on the off-axis factor for a point at a given distance from the central axis of the of the radiation beam 46

C.1 An example of the method of obtaining the average scatter-air ratio from equal sectors centering on a point of interest. Taken from Cundiff, et al. (1973).. 48

ABSTRACT

For most early cases of Hodgkin's disease, radiotherapy is the primary form of treatment and involves the use of large irregularly shaped fields for irradiation of affected lymph node chains. The dosimetry of irregularly-shaped fields is complex and must take into account the variations in radiation exposure across the entire treatment field. To prescribe an optimal course of radiotherapy for a patient with Hodgkin's disease, the radiotherapist must have accurate dosimetry. This study was undertaken to test the accuracy of the dosimetry of a mantle field for treatment of Hodgkin's disease patients at Mary Bird Perkins Cancer Treatment Center. A three-dimensional phantom, or model, of a human thorax was constructed and irradiated with the mantle treatment method. The phantom provided data to compare to doses calculated by three methods: Cundiff, et al. (1973) method, Perkins Cancer Center method, and Capintec Model RT110 computer method. It was found that the method of Cundiff, et al. (1973) was the most accurate for the dosimetry of the mantle field.

CHAPTER ONE

INTRODUCTION

Background Information

The term "malignant lymphoma" includes a spectrum of tumors that originate in the reticuloendothelial system. They were first identified in 1832 by Thomas Hodgkin when he described cases of enlarged lymph nodes not felt to be caused by inflammation. Others had observed the clinical manifestations of the disease, but did not recognize it as a distinct disease process. The manifestations were considered to be the results of other disorders, such as tuberculosis (Kaplan,1972). Toward the end of the nineteenth century, "lymphosarcoma" was distinguished from Hodgkin's disease and from leukemia (Kaplan, 1972). Succeeding years have demonstrated continuing subclassification of the various entities of this leukemia-lymphoma family of diseases.

Hodgkin's disease accounts for 40% of the malignant lymphomas with 50% of Hodgkin's disease cases occuring between the ages of 20 and 40 years (Rubin, 1983);(Figure 1). Typical presentation of the disease is a painless lump which, in 90% of the cases, is supradiaphragmatic with cervical nodes (Figure 2) commonly enlarged in 60 - 80% of these cases; (Rubin,1983). Because of such clinical findings as fever, chills, and leucocytosis, an infectious etiology has been considered as well as ionizing radiation and chemical agents. Thirty-five years ago the average life span for a victim of Hodgkin's

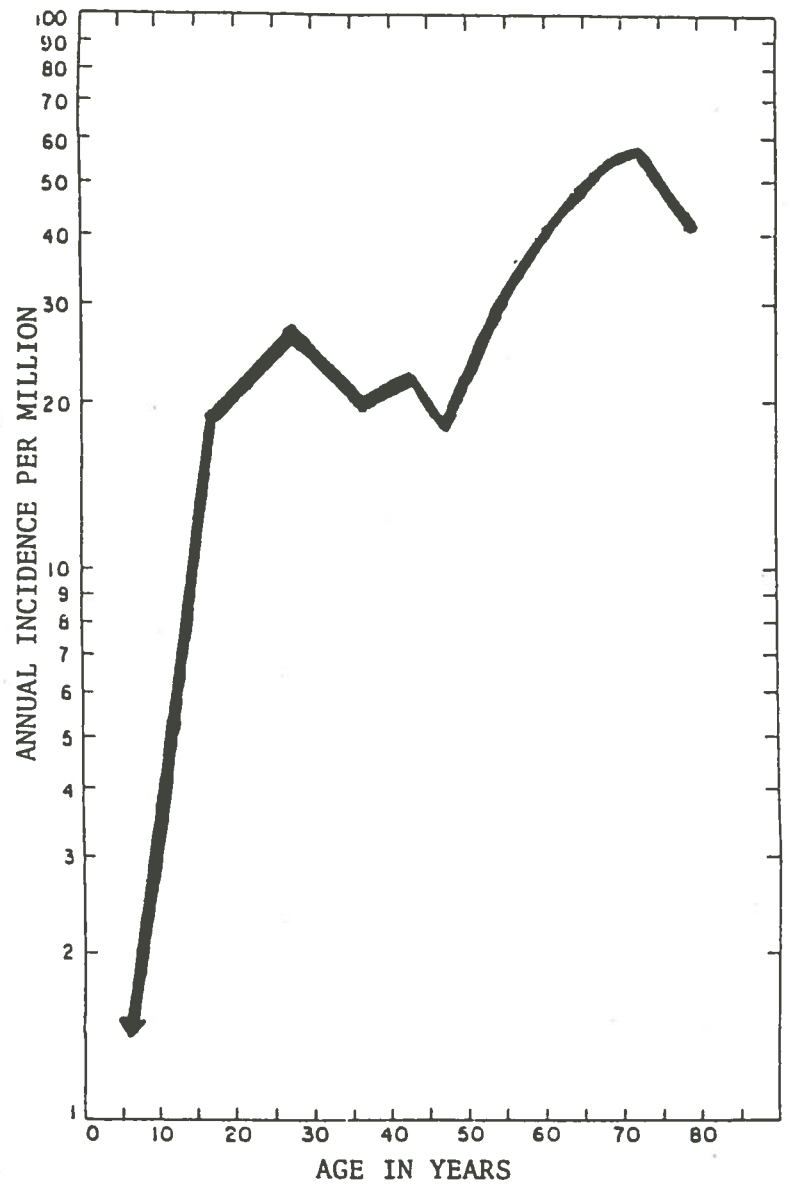

Figure 1. Incidence rates of Hodgkin's disease showing age in years versus incidence per million population. Adapted from Kaplan (1972).

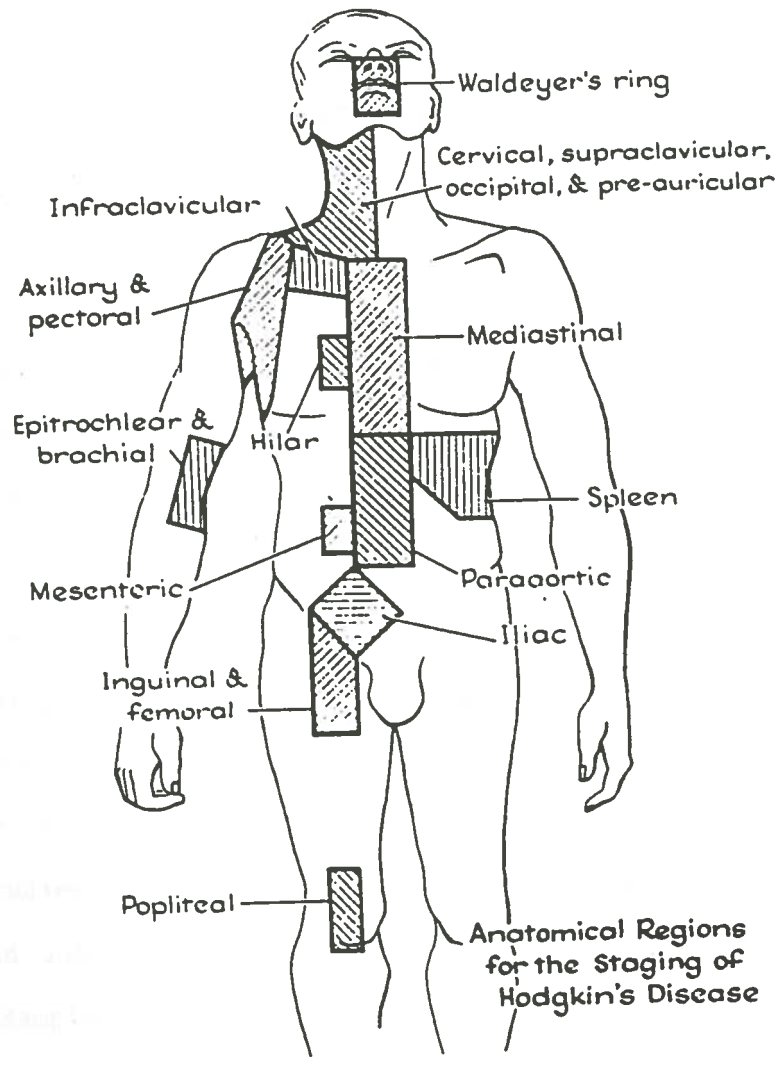

Figure 2. Diagram of the anatomic definition of separate lymph node regions. Taken from Kaplan (1972).

disease was 2.5 years from onset to death; in 1985 the 5-year survival rate was 80-90% and the 10-year survival rate was 60-70% (Lacker, 1985).

Diagnosis and staging (classification of a malignancy for use in prognosis and treatment) is critical in the therapy of Hodgkin's disease because the initial course of treatment offers the best chance for cure. Some lymph node chains are rarely involved, while other chains and extra-lymphatic organs may become involved in a predictable spread of the disease. Contiguous chains of lymph nodes are involved, that is, those chains not necessarily in physical proximity but connected by lymph channels with the para-aortic and iliac nodes serving as a link between the upper trunk and groin (Figure 3). A special contiguity, presumably via the thoracic duct, involves the lower cervical-supraclavicular nodes and upper lumbar-para-aortic with the splenic hilar nodes or spleen or both. Staging is based on clinical studies (e.g., physical findings and history, radiographic studies, and laboratory findings) and surgical-pathological findings for tissue samples from biopsies and laparotomy.

Because an accepted method of staging is important for meaningful communications and as an aid in therapy planning, the 1971 Ann Arbor Symposium on Staging in Hodgkin's Disease recommends a system using both clinical staging and pathological staging (Rubin, 1983). The system consists of :

STAGE I disease in a single node region (I) or a single extra lymphatic organ or site (Ie)

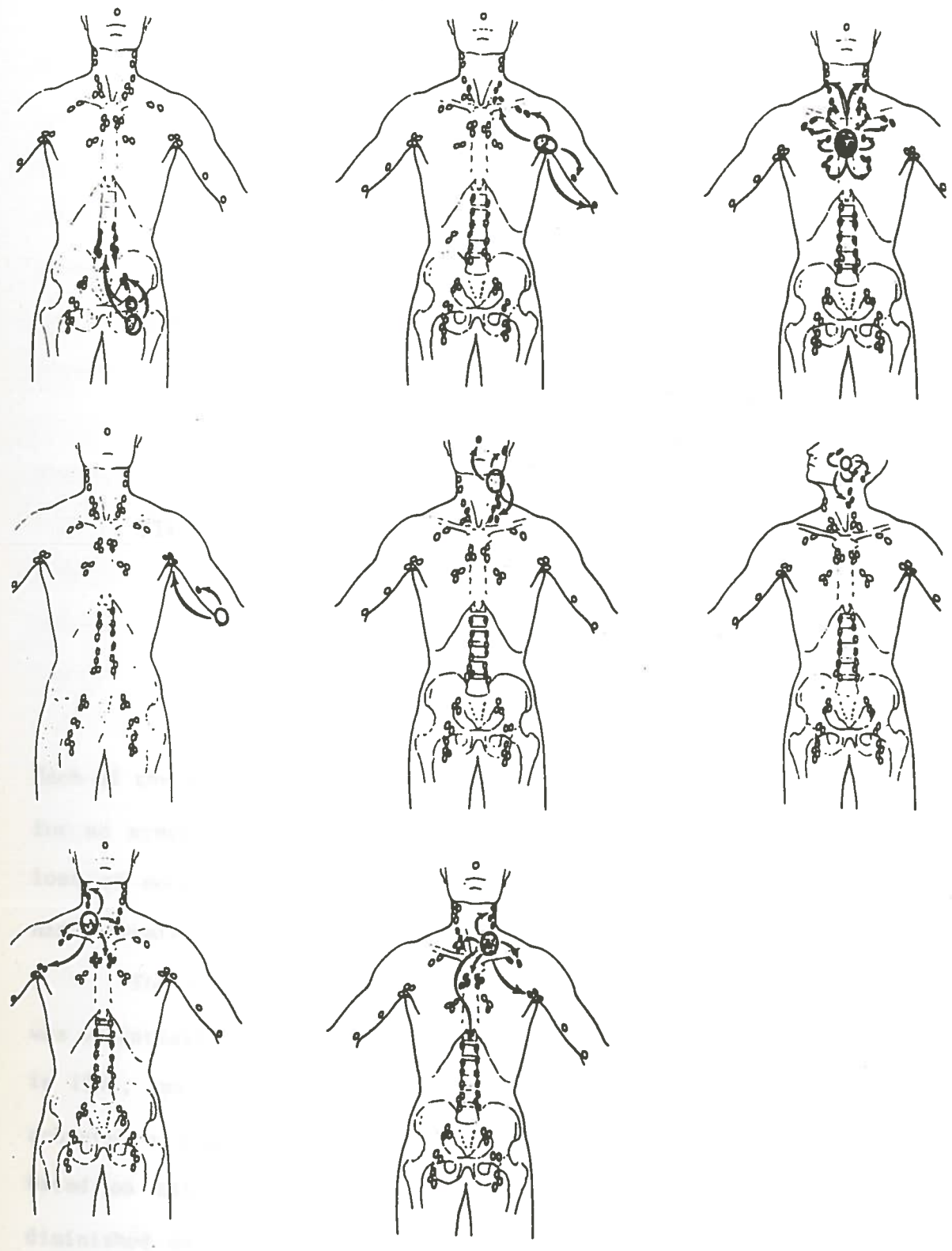

Figure 3. Diagrammatic representation of the pathways of contiguous extension of Hodgkin's disease from various hypothetical primary sites. Taken from Kaplan (1972).

STAGE II — disease in two or more lymph node regions on the same side of the diaphragm (II) or localized involvement of an extralymphatic organ or site and one or more groups of lymph nodes on the same side of the diaphragm (IIe)

STAGE III — diseased lymph node regions on both sides of the diaphragm (III) that may be accompanied by involvement of an extralymphatic organ (IIIe), the spleen (IIIs), or both (IIIse)

STAGE IV — dessiminated disease in one or more extralymphatic organs with or without associated lymph node enlargement; the involved extralymphatic site should be identified by H+ for liver, O+ for bone, D+ for skin, L+ for lung, and M+ for bone marrow.

Each of the above stages is further subdivided into two categories: A for no symptoms or B for generalized symptoms of unexplained weight loss of more than 10% of total body weight, unexplained fevers, or night sweats.

The therapy of Hodgkin's disease and non-Hodgkin's lymphomas was essentially symptomatic throughout the nineteenth century. Pusey in 1902, was apparently the first to treat lymphomas with X-rays and achieved a dramatic reduction in the tumor (Kaplan, 1972). Hopes based on this encouraging initial response, however, were quickly diminished by the apparently unavoidable recurrence of the tumor in the treated area or elsewhere. Interest in the use of radical surgery for eradication of localized lymphomas followed by post-operative

X-ray therapy was high during the period of 1920-1950, but the X-ray therapy alone could have been responsible for the favorable outcomes (Kaplan, 1972). As a by-product of World War II work on compounds related to the mustard gasses, it was found that nitrogen mustards had powerful lymphocytolytic effects on both normal lymphoid tissue and malignant lymphomas. This development marked the beginning of chemotherapy treatment of leukemias and lymphomas.

Current management of Hodgkin's disease and related disorders presents a clear example of the advantage of multidisciplinary collaboration in staging and treatment. Chemotherapy in conjunction with irradiation presents an increased risk of morbidity and is generally used only when systemic symptoms are present with localized disease (e.g., IIB) or for more advanced nodal disease (e.g., III) or when treating recurrences after irradiation (Kaplan, 1972). Radiation therapy is still the primary form of treatment for all early stages of Hodgkin's disease (stages I - IIA). Since the time of Pusey's use of X-rays in the treatment of Hodgkin's disease, the field of radiotherapy has undergone dramatic changes stemming from the invention of reliable machines with higher beam energies, the development of improved techniques for beam alignment and measurement of dose distributions, and the collection of clinical data concerning the mode of origin and the routes of spread of different types of malignancies.

Modern radiation therapy for Hodgkin's disease really began in 1922 with Gilbert (Kaplan, 1962) who was the first to point out certain clinical patterns of the disease and attempt to adapt his

radiotherapeutic techniques to them. He began advocating the irradiation of suspected microscopic disease in apparently uninvolved lymph node chains as well as the clinically-evident sites of disease, emphasizing that the fundamental principle of treatment was to destroy all lesions. He concentrated his efforts on regions known to be diseased then extended the treatment fields to encompass healthy regions "which experience shows more frequently invaded by the process" (Kaplan, 1972). Treatment of these regions involved several adjacent radiation fields.

The dosimetry of field junctions is difficult and complex and presents the possibilty of undertreating lymph nodes or overtreating normal tissues in the vicinity of the field junction. Because errors in dosimetry are more likely to occur when multiple fields are employed, it highly desirable to treat lymph node chains with as few fields as possible (Kaplan, 1962). During the 1950's, a technique of treating the upper torso evolved in which all of the lymph node-bearing areas of the cervicothoracic and axilla regions were treated in continuity by a single radiation portal. The technique has been referred to as the "cervothoracic bath" or, more commonly, the "mantle" field (Figure 4). Common subdiaphragmatic irradiation fields are also illustrated in Figure 4.

The selection of dose in any tumor treatment is an empirical process. For Hodgkin's disease, a megavolt dose of 40-45 Grays (Gy) for involved sites and 30-35 Gy for clinically uninvolved regions are commonly accepted doses (Johnson, 1986), with the total dose being more important than the rate of delivery (Figure 5).

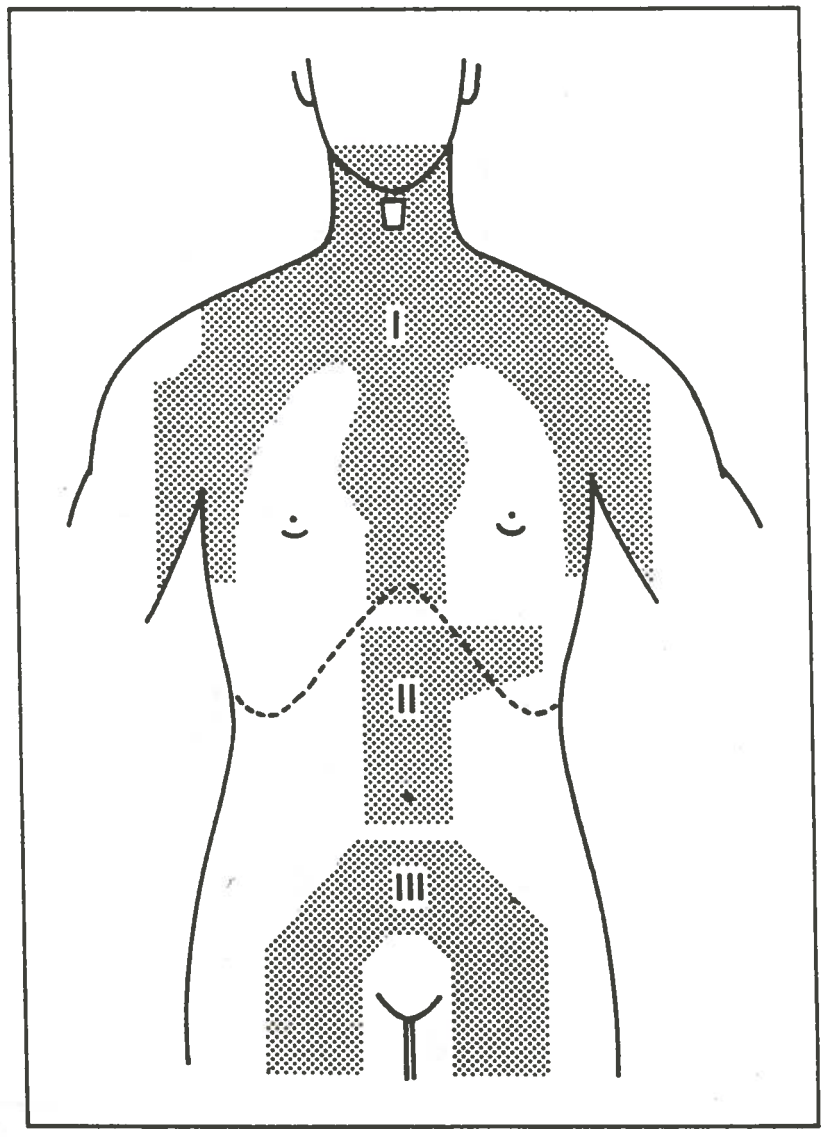

Figure 4. Typical radiation fields commonly employed in Hodgkin's disease. I = mantle field; II = para-aortic-splenic pedicle; III = pelvic. Taken from Rubin (1983).

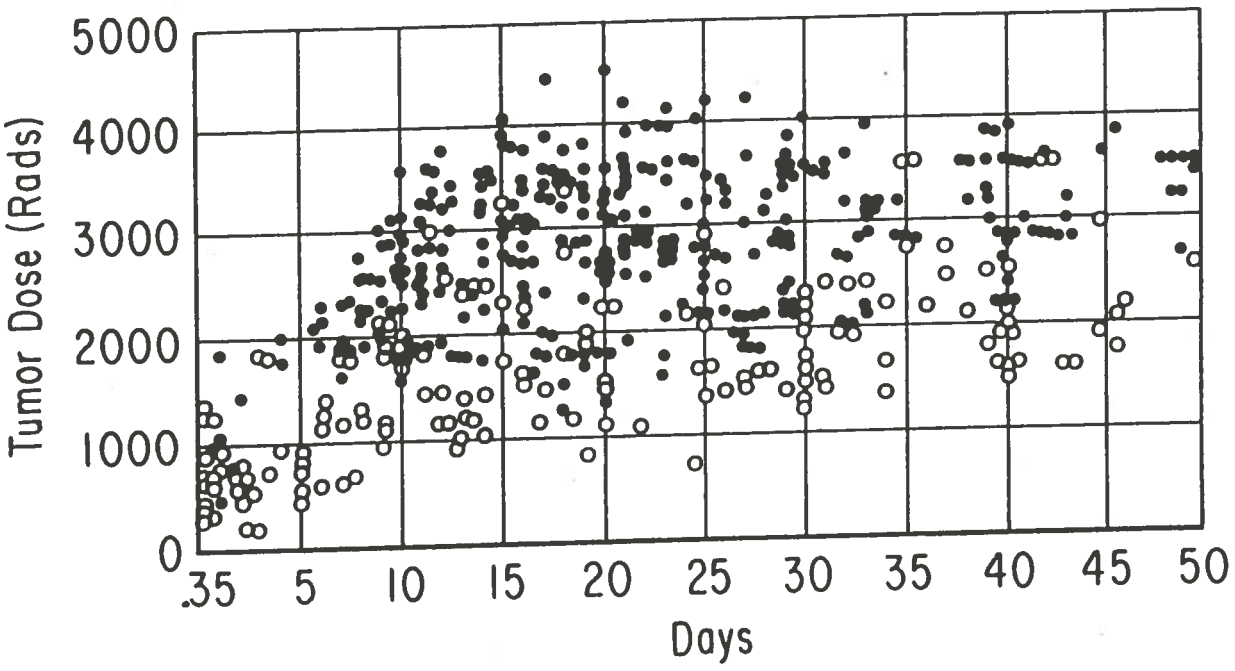

Figure 5. Graph showing the results of different fractionation rates in humans versus total dose. Solid dots signify local tumor control; open dots signify failures. Taken from Fletcher (1980).

Mantle Field Dosimetry

The dosimetry of large irregularly-shaped irradiation fields is complex and is usually an approximation based upon measurements made in a phantom. With small fields of a regular shape, beam characteristics are taken into account in the isodose curves used for dose calculation. In large irregularly-shaped fields for which isodose curves do not exist, beam characteristics must be individually considered when calculating doses.

Two methods of dose calculation are currently used at Mary Bird Perkins Cancer Center in Baton Rouge, Louisiana, (hereafter referred to as Perkins Cancer Center) for the assessment of doses at six points within an anterior mantle field used in the radiotherapy treatment of Hodgkin's disease patients. The points of calculation are the central axis of the field (CAX), and points centered in the regions of the mid-mediastinum, lower mediastinum, axilla, supraclavicular area, and neck (Figure 2). The daily dose for each point is calculated at midline depth (unless otherwise specified by an attending radiotherapist) for a given dose (to depth of dose maximum) of 2 Gy per fraction provided by a 4 MV linear accelerator at a target-to-skin distance (TSD) of 100 cm.

The dose predicting method of Cundiff, et al. (1973) is the basis for the determination of the dose to the CAX, axilla, and neck. This method separates the dose into contributions from the primary beam and from the scattered radiation, with allowances for the variation in exposure and changing TSD across the field. This method

can be used to calculate the dose at any point within the field except within approximately 1 cm of the edges of the field as defined by secondary blocking (Cundiff, et al. (1973)). The primary radiation to a point of interest is dependent upon photon fluence and depth and is determined by using the tissue/air ratio (TAR) for a theoretical "zero" field size. The TAR is defined as the ratio of absorbed dose at a given point in a phantom to the absorbed dose measured at the same point in air within a volume of the phantom material just large enough to provide the maximum electronic buildup at the point of measurement. In this "zero" field size there is considered to be no scatter contribution to the beam. The values for TAR at "zero" field size for a given depth in centimeters (TAR_d) are extrapolated from empirically measured TAR values and are obtained from published tables for a given machine used for treatment.

The dose contribution from scattered radiation depends upon the scatter arising at the field-defining collimators of the linear accelerator and from within the phantom or the patient. Cundiff, et al. (1973) report that the presence of secondary field collimating devices (e.g., the mantle block) may slightly increase or decrease this dose, but the change is usually less than 1% and, therefore, only scatter from the accelerator collimators needs to be considered in the calculation. The scatter/air ratio (SAR) is defined as the difference between the TAR for a given field and the TAR for a zero field size at the same depth. The average SAR for each point of interest at a given depth is calculated by summing the contributions from a number of segments of equal angles (Johns and Cunningham, 1983).

The general calculative formula of Cundiff, et al. (1973), for a fixed TSD is:

$$1.1 \quad D = (Dc * STA)\left(\frac{1}{TARc} * G\right)\left(P * \left[\frac{TSD+e}{TSD+g+d}\right]^2\right)(TARd + SARd)$$

where:

D = dose in cGy at point of interest at depth d in cm

Dc = absorbed dose in a phantom in cGy at depth of dose maximum (given dose) in cm for calibration field size at treatment TSD

STA = blocking tray attenuation factor

TARc = tissue/air ratio for calibration field size at depth in cm of dose maximum

G = field size dependence factor for unblocked treatment field size

P = beam off-axis factor at depth d in cm for the treatment TSD

TSD = target-to-skin distance in cm at the CAX for the treatment field

e = depth in cm of dose maximum

g = vertical distance in cm between skin surface at point of interest and TSD

d = vertical depth in cm from skin surface to point of interest

TARd = tissue/air ratio at depth d for zero field size

SARd = average scatter/air ratio at depth d in cm

The doses calculated according to Cundiff, et al. (1973) for the points at the CAX, axilla, and neck, are compared to the doses determined by a second method of calculation at Perkins Cancer Center. This second method, hereafter refered to as the Perkins method, does not consider the primary and scatter components of the beam independently but does take into account the changes in TSD across the treatment field and the blocked areas of the field. The Perkins method is used as the definitive calculation for doses to the mid-mediastinum, lower mediastinum, and supraclavicular area. The formula consists of:

$$1.2 \quad D = GD * FDD * G * BSF * (TSD/TSDa)^2$$

where:

D = dose in cGy at the point of interest

GD = given dose in cGy for the effective square field size of the blocked treatment field.

FDD = fractional delivered dose for a Clinac 4 at depth of interest, corrected for the increase in treatment TSD by the equation of Hendee (Hendee, 1980)

G = field size dependence factor for unblocked treatment field size

BSF = correction for scatter normalized to calibration field size at depth of maximum dose.

TSDa = target to skin distance for oblique angle from surface point of interest to target; calculated from $[(\text{horizontal distance in cm from CAX})^2+\text{TSD}^2]^{\frac{1}{2}}$

It is the purpose of this thesis to compare the dose prediction method of Cundiff, et al. (1973), the calculative method of Perkins Cancer Center, and computer dose calculations (also based on the Cundiff method (Capintec, (1984)) for points in a mantle field to electrometer readings to determine the accuracy in dose prediction of each method. A stylized (i.e., shape of a human thorax) wax phantom was used to provide dose measurements taken with an ionization chamber to compare with theoretical data.

CHAPTER TWO

MATERIALS AND METHODS

Electrometer readings were taken using a Clinac 4 linear accelerator manufactured by Varian and Associates at a dose rate of 3 Gy/min. The accelerator calibration was verified to be one cGy per monitor unit (MU) (dose setting on accelerator console) at a depth of 5 cm for a 10 cm x 10 cm field at a depth of 5 cm (80 TSD, 200 MU). The electrometer used was a Keithly 614 (SN 312275). A 0.6 cc Farmer chamber probe (SN 435) was used for all readings.

All data used for the Perkins method of dose determination were verified (Appendix A). The off-axis correction factors (used in the Cundiff, et al. (1973) method of calculation) were previously determined at Perkins Cancer Center (Appendix B) using the largest collimator settings on the Clinac 4 and 100 cm TSD (40 cm x 40 cm actual field size). Because the field size for this thesis was smaller than that used in determining the off-axis factors, a ratio of electrometer readings for a given point off the central axis of the beam was determined for varying field sizes and depths.

Because depth-dose data and other factors are traditionally measured in water phantoms, it is necessary to utilize a conversion factor relating a reading in water to a reading in wax so that electromter readings taken in the stylized wax phantom could be converted into a dose in tissue. For the determination of a wax-to-water conversion factor, two identical cube-shaped Lucite^{R} phantoms were used (Figure 6). One was filled with wax and the other

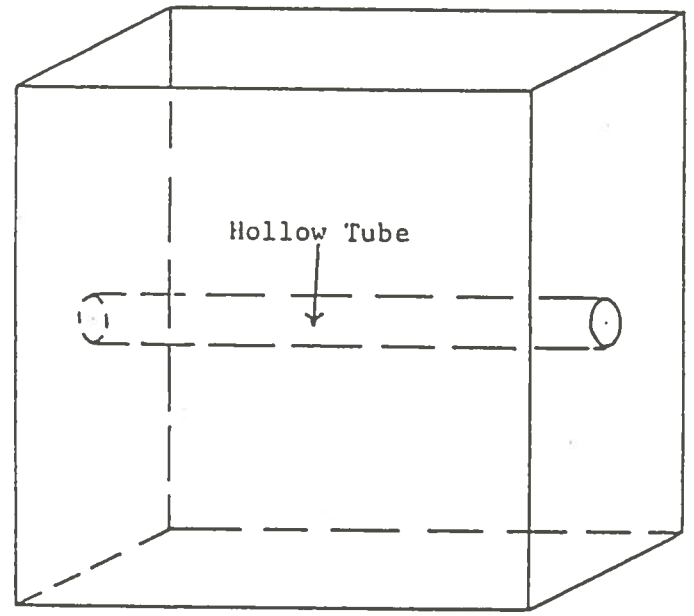

Figure 6. A diagram of the Lucite^{R} cube phantom used to ascertain the water-to-wax conversion factor. Adapted from Nelson (1985).

was filled with water. The phantoms were irradiated using a 10 cm x 10 cm field size and 200 MU at both 80 cm TSD and 100 cm TSD. A wax-to-water conversion factor was found by dividing the average electrometer reading in water by the average electrometer reading in wax.

The shape of the wax phantom for this thesis was contoured from an actual person. A plaster cast extending across the anterior surface of the model and laterally to the top of the radiation treatment table was made of the model's thorax (in the treatment position, described below) using the same type of plaster strips used for casting broken bones. The cast was removed and the inside coated with a washing of plaster of Paris followed by a coating of vegetable oil. The template was then filled with layers of melted wax. After the wax hardened, the plaster cast was removed, leaving a three-dimensional wax phantom of the area irradiated in a mantle field (Figure 7). Points denoting the six areas for dose calculation (CAX, mid-mediastinum, lower mediastinum, axilla, supraclavicular area, and neck) were marked on the surface of the phantom, and the thickness of the phantom at each point was measured. An electrical drill (with a bit having a diameter equal to that of the ionization probe to be used for the measurements) was used to drill into the wax phantom so that the probe could be located at mid-depth directly below each point at marked on the surface of the phantom.

Treatment of an anterior mantle field at Perkins Cancer Center calls for the patient to lie supine on the treatment table with the head resting on a lowered headrest. The patient's hands are placed in

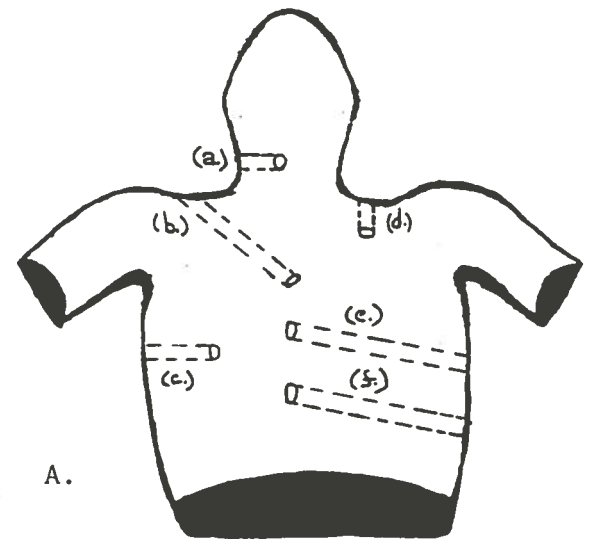

A.

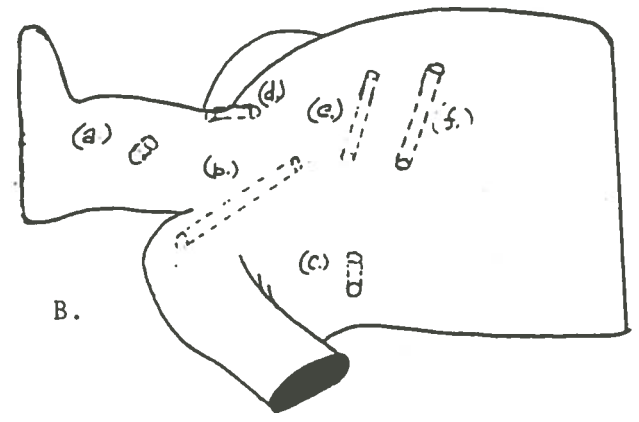

B.

Figure 7. A. A sketch (not to scale) of the wax phantom, viewed from the abdomen to the chin. B. Side view of the wax phantom. Channels for the use of dosimeters are shown as follows: (a) Neck, (b) CAX, (c) Axilla, (d) Supraclavicular, (e) Mid-mediastinum, (f) Lower Mediastinum.

pants pockets, a waistband, or on the patient's waist in such a way as to reproduce the position of the arms as closely as possible for each subsequent treatment. The chin is extended upward and superiorly, and Lucite^{R} sheets are used to raise the head until a carpenter's level shows a parallel line from chin to chest. This is done to minimize the differences in treatment distances across the field as much as possible. The field margins typically extend superiorly along the angle of the mandible, inferiorly across the diaphragm, and laterally to include the entire thoracic width. The field is given its shape by the blocks used to protect the humeral heads and larynx in addition to the characteristically-shaped mantle (lung) block.

The six points of dose calculation are marked on the surface of the patient while in treatment position. Three measurements are taken at each point : the patient thickness, the vertical TSD, and the horizontal distance of the surface point from the central axis. The margins of the blocks are traced directly onto a blocking tray, creating a pattern to be projected by the light field of the linear accelerator. The patient is removed and a large sheet of graph paper is placed on the table. The paper is positioned using the CAX cross-hairs projected by the light field of the linear accelerator. The table is raised to a distance equal to one-half of the patient's thickness at the central axis point, thus illuminating on the paper the field pattern at the patient's mid-depth. This pattern is later used to calculate the average scatter/air ratio for each point of dose assessment.

The wax thoracic phantom, so constructed as previously described, was placed upon the treatment table, and a carpenter's level was used to check the horizontal position of the chin. The TSD at the CAX was set at 100 cm and the collimators of the accelerator set at 27 x 30 to produce the field margins discussed previously. The mantle block, larynx block, and humeral head blocks were positioned on a blocking tray and the pattern was traced onto the blocking tray prior to irradiation. The pattern illuminated by the accelerator light field was later traced onto graph paper as described.

A lead bead was placed on the surface of the phantom at each point of dose calculation and a metal wire was positioned in each channel. The alignment of the channel drilled into the thoracic phantom in relation to the point of interest marked on the surface was then verified radiographically. The depth of the center of the probe in the channel was determined from radiographs taken laterally of each marked point. A brass ring of known diameter (i.e., magnification ring) was placed around the bead marking the interest point for each film. The apparent diameter of the ring versus its known diameter is used to correct for the magnification of the film. The depth of the probe in each drilled channel predicted from phantom thickness measurements was corrected, for dose calculations, to the actual depth of the probe when placed in each of the drilled channels.

Irradiation of the wax phantom was done on the Clinac 4 linear accelerator using a machine setting of 312 MU, as routinely used on Hodgkin's patients at Perkins Cancer Center. A 0.6 cc Farmer chamber probe was placed sequentially in each drilled channel and 5

electrometer readings were taken at each point. The first reading of each set was discarded according to protocol (Kubricht, 1986), and the remaining four readings were averaged for each point of calibration at depth. The averaged electrometer readings were converted to cGy using the following equation (Linac Calibration, 1984) :

$$2.1 \qquad D_t = R*N*C* C_t * C_p * C_{ch} * C_{max} * C_{water}$$

where:

D_t = dose in cGy in tissue

R = electrometer reading in Coulombs

N = chamber factor in Roentgen/Coulomb

C = Roengten to cGy conversion factor

C_t = temperature correction factor

C_p = pressure correction factor

C_{ch} = charge correction factor

C_{wax}= wax-to-water correction factor

C_{water}= water-to-tissue correction factor

The average SAR for each point was determined by the method detailed by Cundiff, et al. (1973);(Appendix C). The average SAR for each of the six points of calculation was also determined by the Capintec Model RT110 computer. The Capintec computer also generated dose calculations at each of the six points using the irregular field option.

CHAPTER THREE

RESULTS

The fractional depth dose for the Clinac 4 linear accelerator was found to be within $\pm$ 1.0% of the published data of Peterson and Golden (1972). This published data for fractional depth doses are routinely used for dose assessment at Perkins Cancer Center and in this thesis (Appendix A). Values for field size dependence and backscatter factors (described in formulas 1.1 and 1.2) were found to be within $\pm$ 1% of the data used at Perkins Cancer Center; the latter data were used by the author for calculations (Appendix A). It was found that decreasing the field size from that used for the determination of off-axis correction factors produces a slightly decreased value for a given point (Appendix B).

The conversion factor to relate a dose in wax to a dose in water was determined using two identical Lucite^{R} phantoms, one filled with water and the other filled with wax. Previous comparison of the electrometer readings from each phantom showed that the average electrometer reading in water was 98.3% of the average electrometer reading in wax, when irradiated with a 10 cm x 10 cm field size, (80 cm TSD and 200 MU);(Nelson, 1985). Extension of the TSD to 100 cm showed no change in the ratio of electrometer readings in wax to the electrometer readings in water. Because readings taken in the wax phantom were higher than readings taken in the water phantom, all readings taken in the wax thoracic phantom were multiplied by a factor

Table 1. Table of the measurement distances in cm used for dose calculation by the Perkins method. These distances were determined by measurement of the thoracic wax phantom.

MEASUREMENTS USED TO DETERMINE DOSES

POINT OF CALCULATION	TSD	DISTANCE OFF CAX	PHANTOM THICKNESS	DEPTH OF PROBE
CAX	100.0	0.0	9.5	5.8
MID-MEDIASTINUM	97.3	5.0	11.5	5.6
LOWER MEDIASTINUM	96.2	12.5	12.5	6.2
AXILLA	101.0	17.5	8.5	3.0
SUPRACLAVICULAR AREA	102.0	8.5	7.5	3.0
NECK	103.0	12.0	6.5	2.8

Table 2. The SAR for each point of calculation in the thoracic wax phantom as determined by the Capintec computer compared to the SAR for each point as determined by manual averaging, detailed by Cundiff, et al. (1973).

SCATTER/AIR RATIOS

POINT OF DETERMINATION	CAPINTEC	MANUAL
CAX	0.212	0.209
MID-MEDIASTINUM	0.197	0.207
LOWER MEDIASTINUM	0.138	0.134
AXILLA	0.100	0.098
SUPRACLAVICULAR AREA	0.129	0.125
NECK	0.106	0.112

Table 3. Comparison of actual tissue dose (A) in cGy to the predictions of tissue dose in cGy by the Perkins method (B), the Cundiff, et al. (1973) method (C), and the Capintec computer method (D).

POINT OF CALCULATION	DOSE IN cGy* A	B	C	D
CAX	165	166	166	167
MID-MEDIASTINUM	182	181	180	178
LOWER MEDIASTINUM	183	173	175	160
AXILLA	194	180	195	178
SUPRACLAVICULAR AREA	198	180	192	183
NECK	187	176	188	179

*A = from elecrometer readings
B = from Perkins method
C = from Cundiff, et al. method
D = from Capintec computer

patients are presented in Table 4.

Table 4. Comparison of the predictions of tissue dose in cGy in patients by the Perkins method (A) and the method of Cundiff, et al. (1973) (B).

DOSES IN cGy

PATIENT	CAX[a] A	CAX[a] B	MID-MED[b] A	MID-MED[b] B	LOW MED[c] A	LOW MED[c] B	AXILLA A	AXILLA B	SC AREA[d] A	SC AREA[d] B	NECK A	NECK B
A	160	160	157	164	155	149	165	174	180	188	174	183
B	151	153	141	145	137	139	149	156	151	160	161	165
C	145	147	141	145	143	144	151	156	182	182	164	170
D	157	158	148	150	143	136	156	161	180	192	167	173
E	145	146	142	166	140	137	148	151	175	186	176	186
F	160	161	151	156	151	149	162	169	180	189	172	182
G	158	162	149	157	157	163	157	160	164	176	173	181
H	158	160	155	160	153	149	166	170	182	191	166	176
I	157	161	152	159	148	147	161	171	164	178	171	180

a=central axis

b=mid-mediastinum

c=lower mediastinum

d=supraclavicular area

A = Perkins method of calculation

B = Cundiff,et al.(1973) method of calculation

CHAPTER FOUR

DISCUSSION

The use of published depth dose data for a Clinac 4 linear accelerator (Peterson and Golden, (1972)) is an acceptable and widely practiced policy, provided that the data from the individual accelerator are comparable. The empirical determination of depth dose data, field size dependence factors, backscatter factors, and off-axis factors are generaly done in rectangular water-filled phantoms that give very uniform isodose curves. Irradiation of irregularly-shaped objects, such as people, will result in irregularly shaped isodose curves.

When examining the doses of calculation generated by the Perkins method of calculation it is noted that, except for the CAX, the doses are underestimated. The doses were underestimated by a minimum of 1.1 % (mid-mediastinum) and a maximum of 10 % (supraclavicular area). The author feels that the Perkins method should not be the definitive calculation for the dose at any point in the mantle field , with the exception of the CAX. Because the CAX is at the center of the radiation field, off-axis factors and altered TSD need not be accounted for, thus reducing the introduction of error into the calculation. The effects of scatter on the dose at this point are handled reasonably well by the field size dependence and backscatter factors due to the relatively uniform distribution of the field around the point.

The doses predicted by the Cundiff, et al. (1973) method are also underestimated (excluding the CAX) when compared to actual measurements, but to a lesser degree than the Perkins method of calculation. Comparison of the Cundiff, et al. (1973) and the Perkins methods of calculation shows the Cundiff method to consistently (except for the CAX and lower mediastinum) predict higher doses. The major discrepancy in the doses predicted by the Cundiff method and actual measurements for the wax phantom occurs at the lower mediastinum : the dose calculated is 4.6% lower than the measured dose. For the irradiation of the thoracic wax phantom, the point denoting the lower mediastinum was marked approximately one centimeter from the inferior field margin as defined by the mantle block. As pointed out by Cundiff,et al. (1973), his method of calculation does not accurately predict dose at a point within this region of the field margin. The differences between actual delivered dose at each of the six points and the doses predicted for these points by Cundiff's method were summed. An average percent difference of 1.7 %, generalized to include all six points, was determined. This small percent difference indicates that the method of Cundiff,et al. (1973) is acceptably accurate for calculation of doses within a mantle field.

Comparing the measured doses to those generated by the Capintec computer shows the Capintec to also underestimate the doses to the points of calculation. Examination of a dose analysis table produced by the Capintec computer shows the off-axis correction factors used by the computer are lower than those read from the graphs in Appendix B. Although the graphed values of the off-axis correction

factors used in the Cundiff method are larger than the values for the actual field size used on the phantom, the per cent difference is small (less than 2.5%), and use of the larger graphed value in the Cundiff method is acceptable (Kubricht, 1986). Increasing the doses generated by the computer by the per cent difference in the off-axis factors of the computer versus those graphed for Perkins Cancer Center does elevate the computer value. The doses calculated by the Cundiff method however, are still closer to the measured radiation doses.

Comparison of the three methods of dose calculation to each other and to the measured doses indicates the Cundiff, et al. (1973) method demonstrates the greatest accuracy in dose prediction. The Cundiff method should be used as the definitive calculation of doses to the six regions of interest in a mantle field. The Capintec computer can, however, be used for the assessment of the average SAR at each point of interest, thus expediting the dose analysis at points within a mantle field.

REFERENCES

1. Anderson, R.E., D'Angio, G.J., Khan, F.M. (1969). Dosimetry of irregularly shaped radiation therapy fields (Parts I and II). Radiology 92:1092-1100.

2. Boge, R.J., Tolbert, D.D., Edland, R.W. (1985). Accessory beam flattening filter for the Varian Clinac 4 linear accelerator. Radiology 115:475-477.

3. Capintec Computer Operators Manual, Capintec Industries Incorporated. (1984).

4. Clarkson, J.R. (1941). A note on depth doses in fields of irregular shape. British Journal of Radiology 14:265-268.

5. Clarkson, J.R., Herbert, R.J. (1948). Surface and emergent doses in radiotherapy. British Journal of Radiology 21:494-500.

6.. Cundiff, J.H., Cunningham, J.R., Golden, R., Lanze, L.H., Meurk, M.L., Ovadia, J., Last, V.P., Pope, R.A., Samphere, V.A., Saylor, W.L., Shalek, R.J., Suntharalengham,N. (1973). A method for the calculation of dose in the radiation treatment of Hodgkin's disease. American Journal of Roentgenology, Radium Therapy, and Nuclear Medicine 67: 30-44, January 1973.

7. Cunningham, J.R., Johns, H.E., Gupta, S.K. (1965). An examination of the definition and magnitude of back-scatter factor for cobalt-60 gamma rays. British Journal of Radiology 38: 637-638.

8. Doppke, K.P. (1983) Advances in radiation therapy treatment planning. Medical Physics, monograph 9.

9. De Vita, V.T., Canellos, G.P., Moxley, J.H. (1972). A decade of combination chemotherapy of advanced Hodgkin's disease. Cancer 30:1495-1504.

10. Ellis, F., Hall, E.J., Oliver, J. (1959). A compensator for variations in tissue thickness for high energy beams. British Journal of Radiology 32:421-422.

11. Faw, F.L., Johnson, R.E., Warren, C.A., Glen, D.W. (1971). A standard set of "individualized" compensating filters for mantle field radiotherapy of Hodgkin's disease. American Journal of Roetgenology, Radium Therapy, and Nuclear Medicine 111:376-381.

12. Fletcher, G.H. (1980). Textbook of Radiotherapy, Third Edition. Lea and Febiger; Philadelphia, pp. 959.

13. Gagnon, W.F., Grant, W. (1975). Surface dose from megavoltage therapy machines. Radiology 117:705-708.

14. Gilbert, R. (1939). Radiotherapy in Hodgkin's disease (malignant granulomatosis) American Journal of Roengtenology, Radium Therapy, and Nuclear Medicine 41:198-241.

15. Gray, L., Prosnitz, L.R. (1975). Dosimetry of Hodgkin's disease therapy using a 4MV linear accelerator. Radiology 116:423-428.

16. Gray, L., Prosnitz, L.R. (1975). Mantle field dosimetry comparing 4MV with cobalt-60. Radiology 116:429-432.

17. Gupta, S.K., Cunningham, J.R. (1966). Measurement of tissue air ratios and scatter functions for large field sizes, for cobalt-60 gamma radiation. British Journal of Radiology 39: 7-11.

18. Hansen, H.H., Conner W.G., Doppke, K., Boone, M.L. (1972). A new field flattening filter for the Clinac-4. Radiology 103: 443-446.

19. Hendee, W. (1980). Medical Physics Radiology Second Edition. Holt, Rinehart, and Winston; New York, New York. pp.464.

20. Holt, J.G., Laughlin, J.S., Meroney, J.P. (1970). The extension of the concept of tissue-air ratios (TAR) to high energy X-ray beams. Radiology 96:437-446.

21. Johns, H.E., Cunningham, J.R. (1983). The Physics of Radiology Fouth Edition. Charles C. Thomas; Springfield, Illinois. pp. 796.

22. Johnson, S. (1986). Mary Bird Perkins Cancer Center (Personal communication.)

23. Kaplan, H.S. (1962). The radical radiotherapy of regionally localized Hodgkin's disease. Radiology 78:553-561.

24. Kaplan, H.S. (1972) Hodgkin's Disease. Harvard University Press, Cambridge, Massachusetts. pp 452.

25. Kubricht, W.S. (1986). Mary Bird Perkins Cancer Center (Personal communication.)

26. Lacker, M.J. (1985). Hodgkin's disease : historical perspective, current status and future directions. CA - A Cancer Journal for Clinicians (American Cancer Society) 35:88-94.

27. Lane, R.G., Paleival, B.R. (1975). Extended field treatment flattness filter for 4 MV linear accelerators. Radiology 115:478-479.

28. Levitt, S.H., Bloomfield, C.D., Lee, C.K., Nesbit, M.E., McKenna, R.W. (1976). Extended field radiotherapy in non-Hodgkin's lymphoma. Radiology 118:457-459.

29. Linac Calibration Protocol, Mary Bird Perkins Radiation Treatment Center, Baton Rouge, Louisiana. Revision of 1/84.

30. Mc Cullough, E.C., Earle, J.D. (1982). A measurement of doses to the neck for mantle field treatment of lymphomas with cobalt-60, 4 -, and 10 - MV photon. Radiology 144:432-434.

31. Meurk, M.L., Green, J.P., Nussbaum, H., Vaeth, J.M. (1968). Phantom dosimetry study of shaped coblt-60 fields in the treatment of Hodgkin's disease. Radiology 91:554-558.

32. Maruyama, Y., Khan, F.M. (1971). Blocking considerations in mantle therapy. Radiology 101:167-173.

33. Nelson, G.E. (1985). Inconsistencies of Traditional Breast Dosimetry, Masters Thesis.

34. Page, V., Gardner, A., Karzmark, C.J. (1970). Physical and dosimetric aspects of radiotherapy of malignant lymphomas I : The mantle technique). Radiology 96:609-618.

35. Peters, M.V. (1950). A study of survivals in Hodgkin's disease treated radiologically. The American Journal of Roengtenology and Radium Therapy. Radiology 63:299-311.

36. Peters, M.V., Middlemiss, K.C. (1958). A study of Hodgkin's disease treated by irradiation. American Journal of Roentgenology, Radium Therapy, and Nuclear Medicine 79: 114-121.

37. Peterson, M., Golden, R. (1973). Dosimetry of the Varian Clinac-4. 1. Basic radiation parameters. Radiology 103: 675-680.

38. Rosenberg, S.A., Kaplan, H.S. (1975). The management of stages I,II, and III Hodgkin's disease with combined radiotherapy and chemotherapy. Cancer 35:55-63.

39. Rubin, P., Kurohara, S.S. (1966). Has prophylactic irradiation proved itself in the treatment of localized Hodgkin's disease? Radiology 87:240-252.

40. Rubin, P. (1983) Clinical Oncology for Medical Students and Physicians:A Multidisciplinary Approach, Sixth Edition. American Cancer Society; Rochester, New York pp 536.

41. Werner, B.L., Khan, F.M., Lee, C.K., Levitt, S.H. (1981). Choice of beam energy for mantle - field radiotherapy of malignant lymphoma. Radiology 141:795-795.

APPENDIX A

DATA FOR PERKINS METHOD OF CALCULATION

All data currently in use for dose calculation according to the Perkins method was verified. A 40 cm x 40 cm thin-window Lucite^R water phantom was irradiated (80 cm TSD, 200 MU) to obtain electrometer readings for depths at chosen field sizes. The electrometer reading for each depth was normalized to electrometer reading at the depth of maximum dose (D max) for a given field size. The resulting ratios are the fractional delivered doses for each field size (Figure A.1). The same phantom, with the probe fixed at the depth of dose maximum (1.2 cm), was irradiated (80 cm, 200 MU) to obtain electrometer reading at various field sizes. Each reading was normalized to the electrometer reading for the 10 cm x 10 cm field size to give output factors for varying field sizes (Figure A.2).

The probe was covered with a Lucite^R buildup-cap (radius 1.3 cm) and positioned at 80 cm TSD for irradiation (200 MU) at varying field sizes. Normalization of the electrometer readings at each field size to a 10 cm x 10 cm field gives field size dependence correction factors for varying field sizes (Figure A.3). The backscatter factor (BSF) for a given field size was calculated from the output factor for that field size divided by the field size dependence correction factor for the same field size. The backscatter factors are graphed versus varying field sizes (Figure A.4).

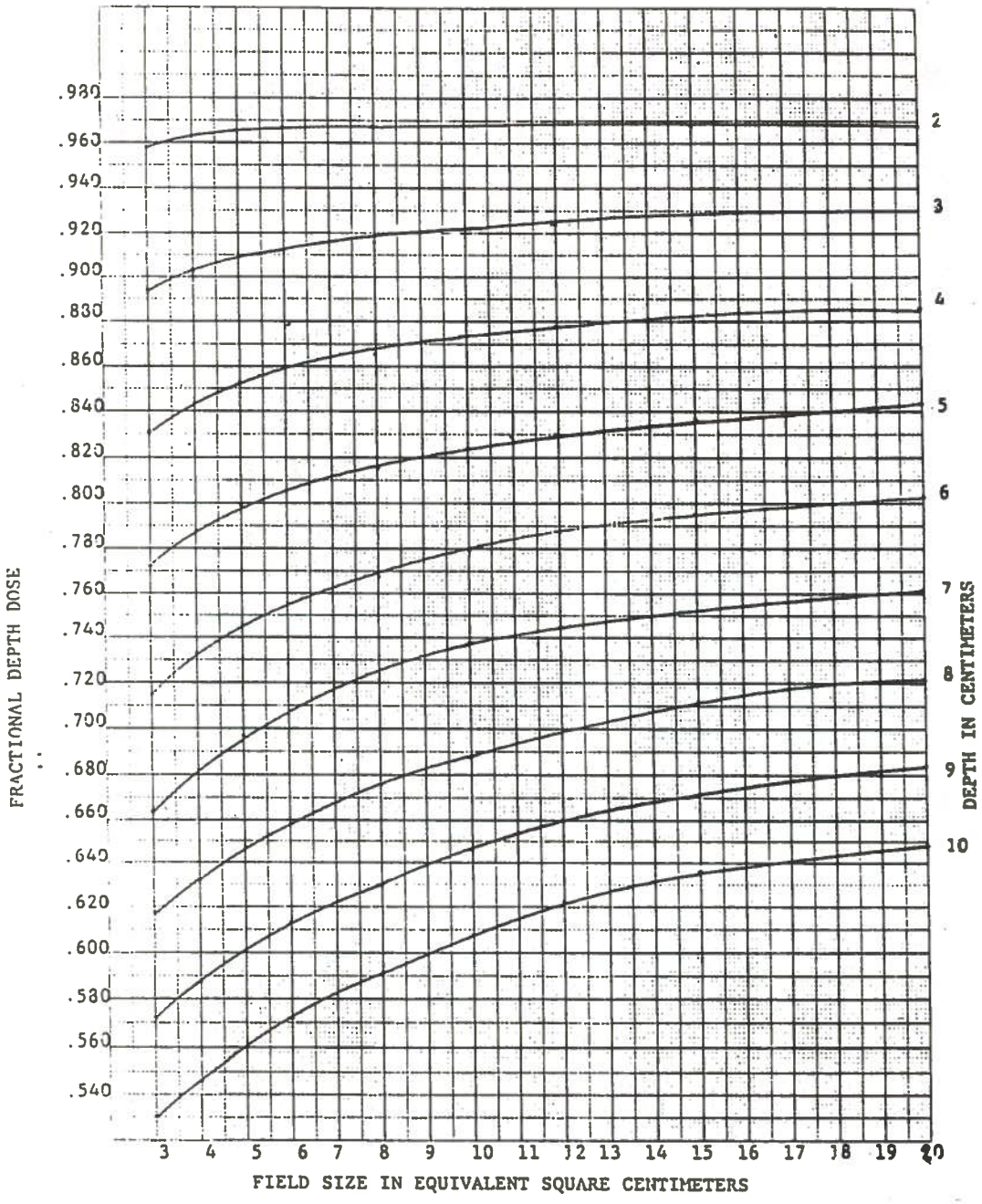

Figure A.1 Fractional depth dose for increasing field sizes and depths in cm for the Clinac 4 linear accelerator (Peterson and Golden, 1972).

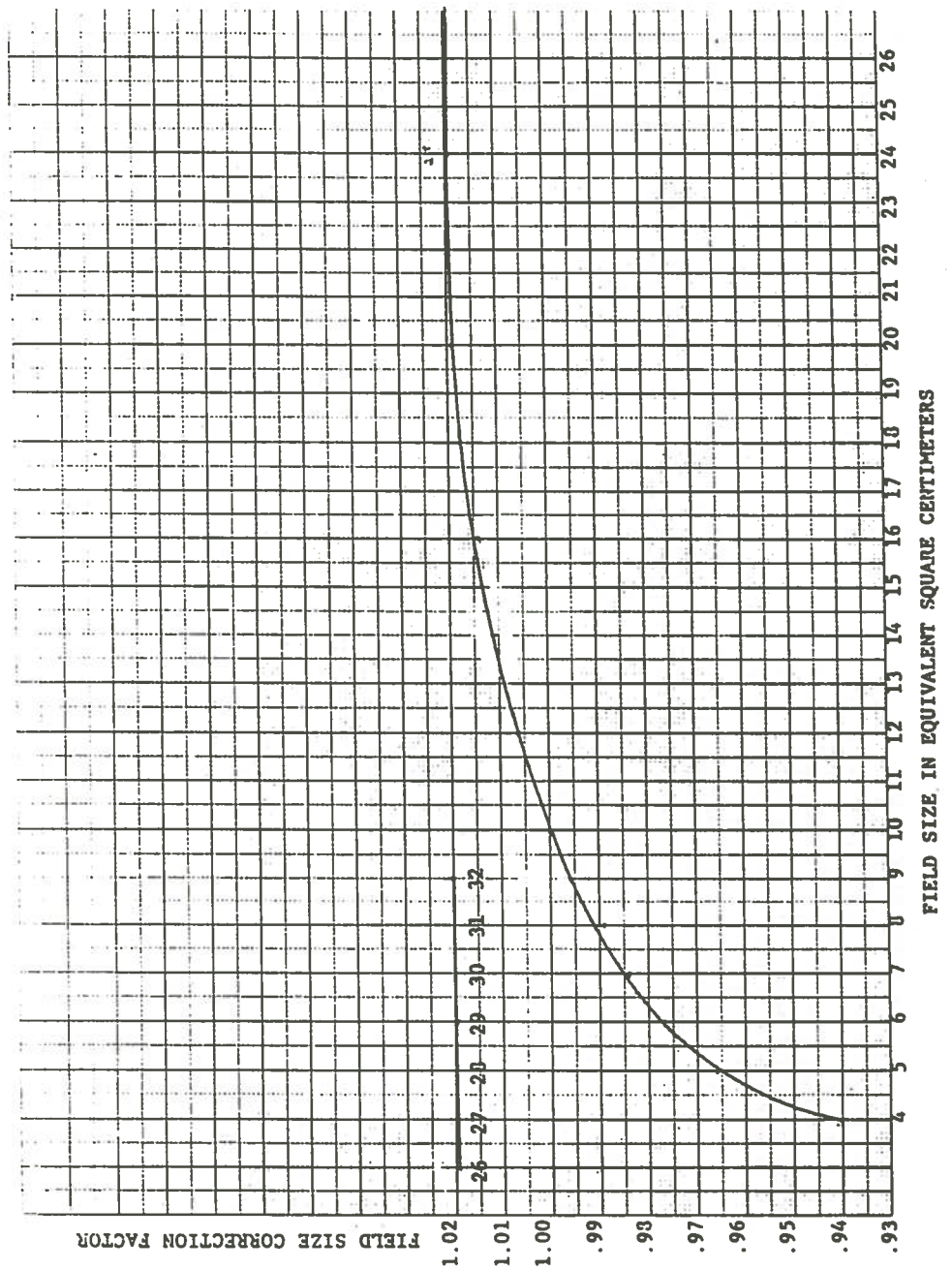

Figure A.2 Output correction factors for increasing field sizes in cm for a Clinac 4 linear accelerator at Perkins Cancer Center (Kubricht, 1986).

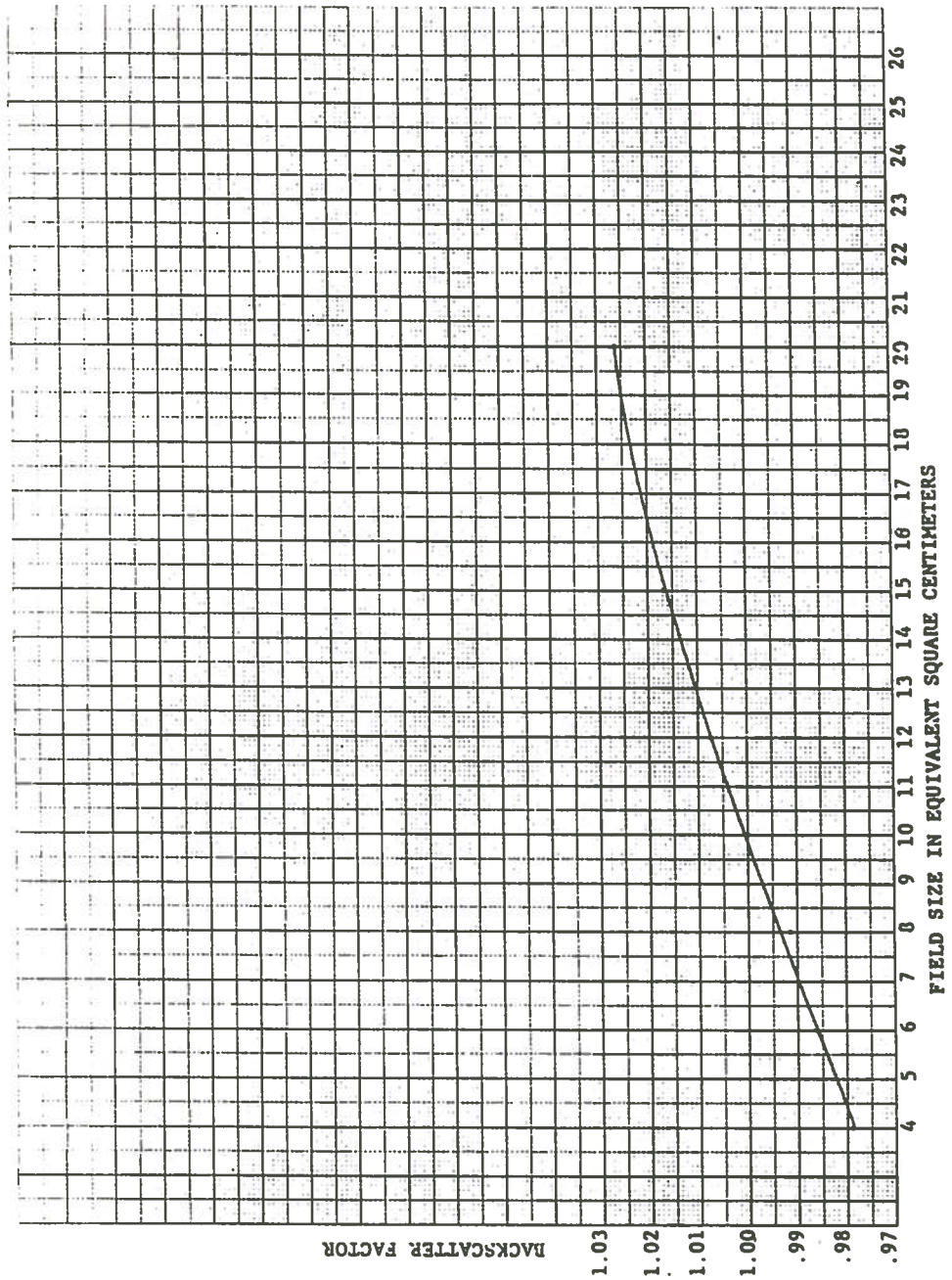

Figure A.3 Field size dependence correction factors for a Clinac 4 linear accelerator at Perkins Cancer Center (Kubricht, 1986).

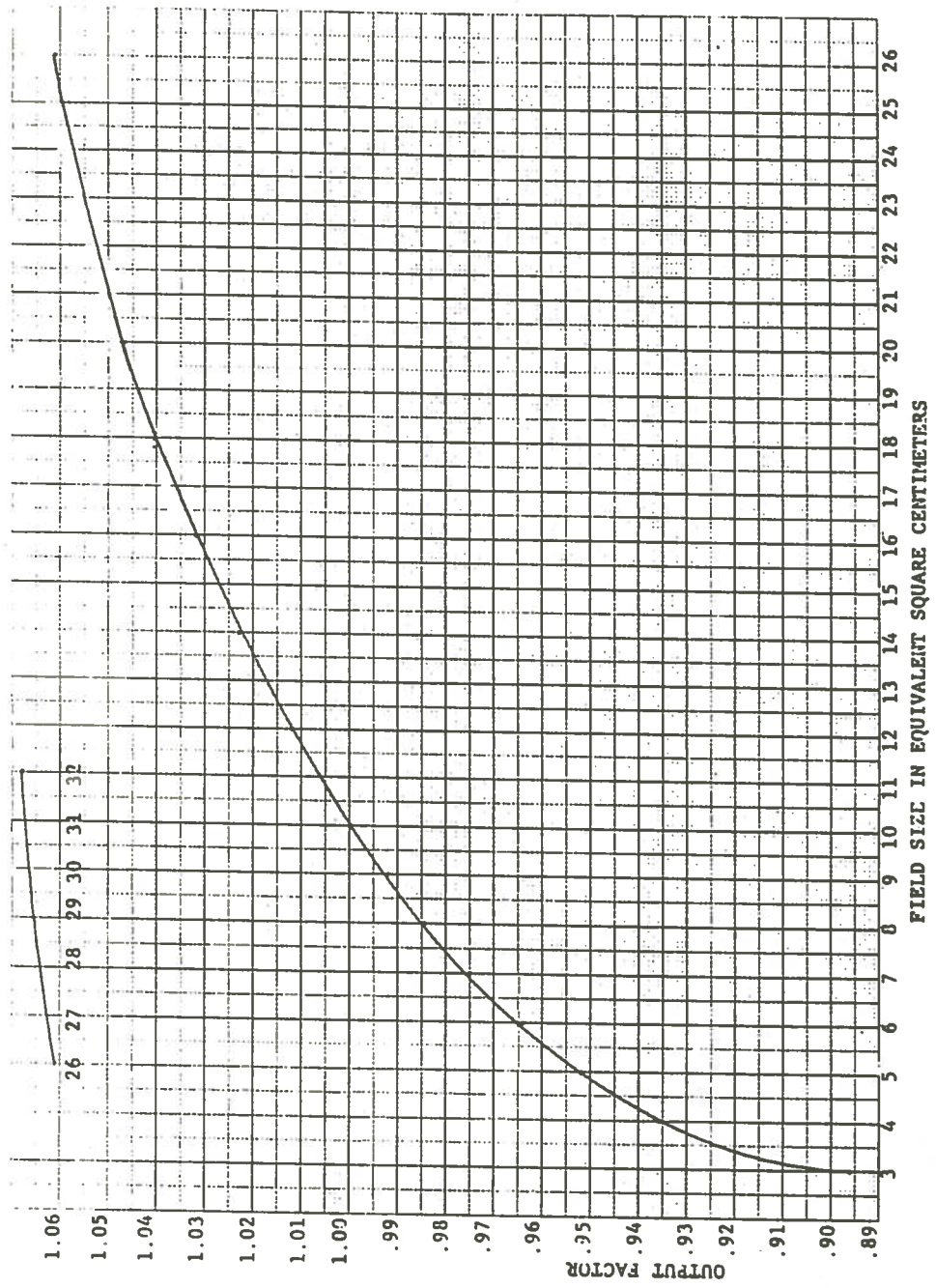

Figure A.4 Backscatter correction factors for a Clinac 4 at Perkins Cancer Center (Kubricht, 1986).

APPENDIX B

OFF-AXIS FACTORS

The Clinac 4 linear accelerator employs a beam flattening filter designed in most instances to produce a flat isodose distribution at 10 cm depth with emphasis on small field sizes. When larger fields are used, areas of higher dose occur at the lateral beam edges espically near the surface of the irradiated object. The presence of these "horns" of higher radiation are corrected for in dose calculations by a ratio of the amount of radiation at a point off the central axis of the beam to the amount of radiation at the central axis. This correction ratio is called an off-axis factor and its magnitude for a given point is affected by the distance of the point from the central axis (CAX), the depth of the point in the phantom or the patient, and the accelerator used for irradiation. Figures B.1, B.2, and B.3 are graphs of the off-axis factor versus the distances in cm off CAX for three different depths. The effect of depth and collimator setting on the value of the off-axis factor for a point 12 cm from the CAX was evaluated. The difference in off-axis factors at a given depth for three collimator settings is expressed as a per cent change in Figure B.4.

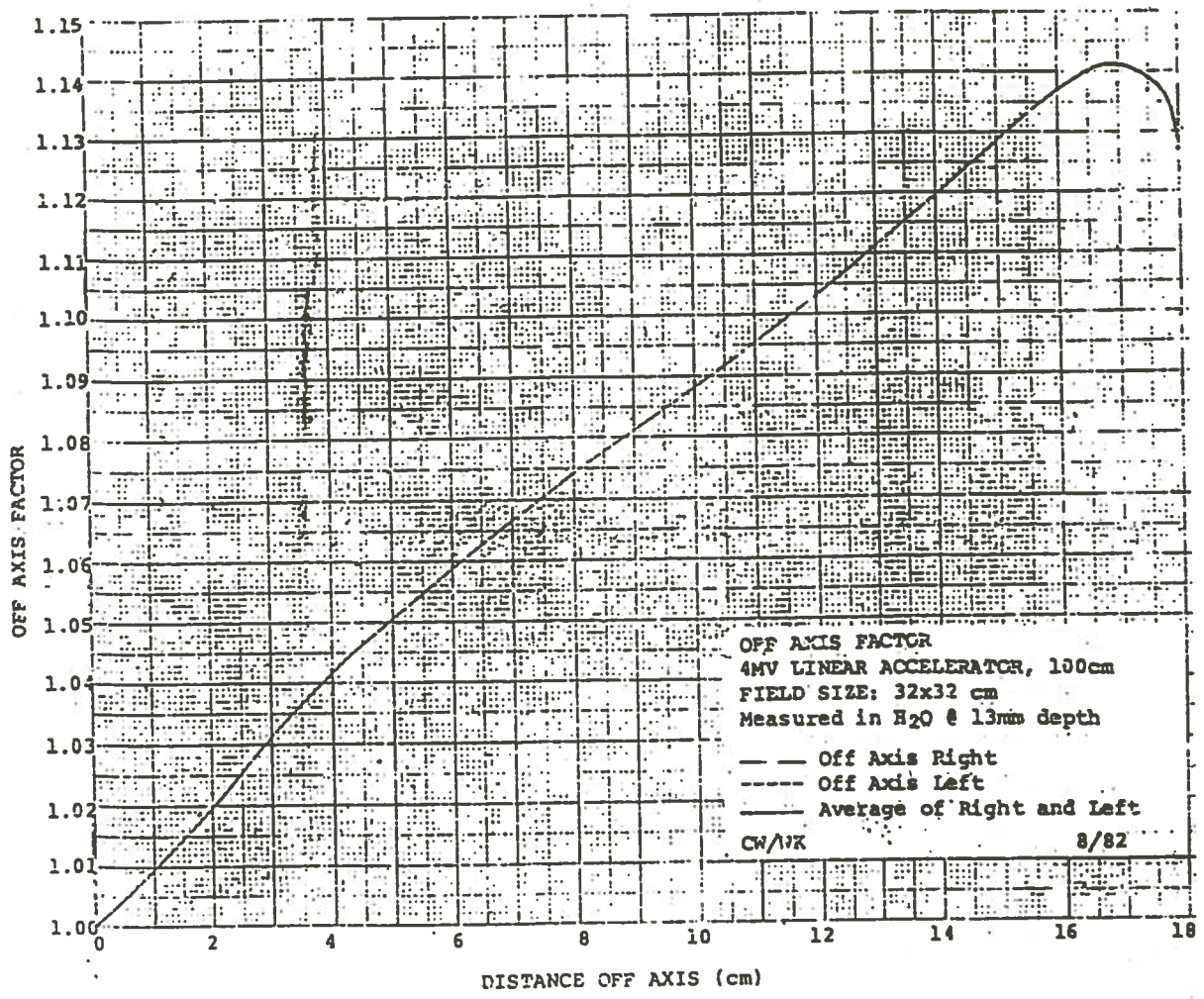

Figure B.1 Graph of the relationship between the off-axis factor and the distance in cm off the central axis, measured in water at a 13 mm depth (Kubricht, 1986).

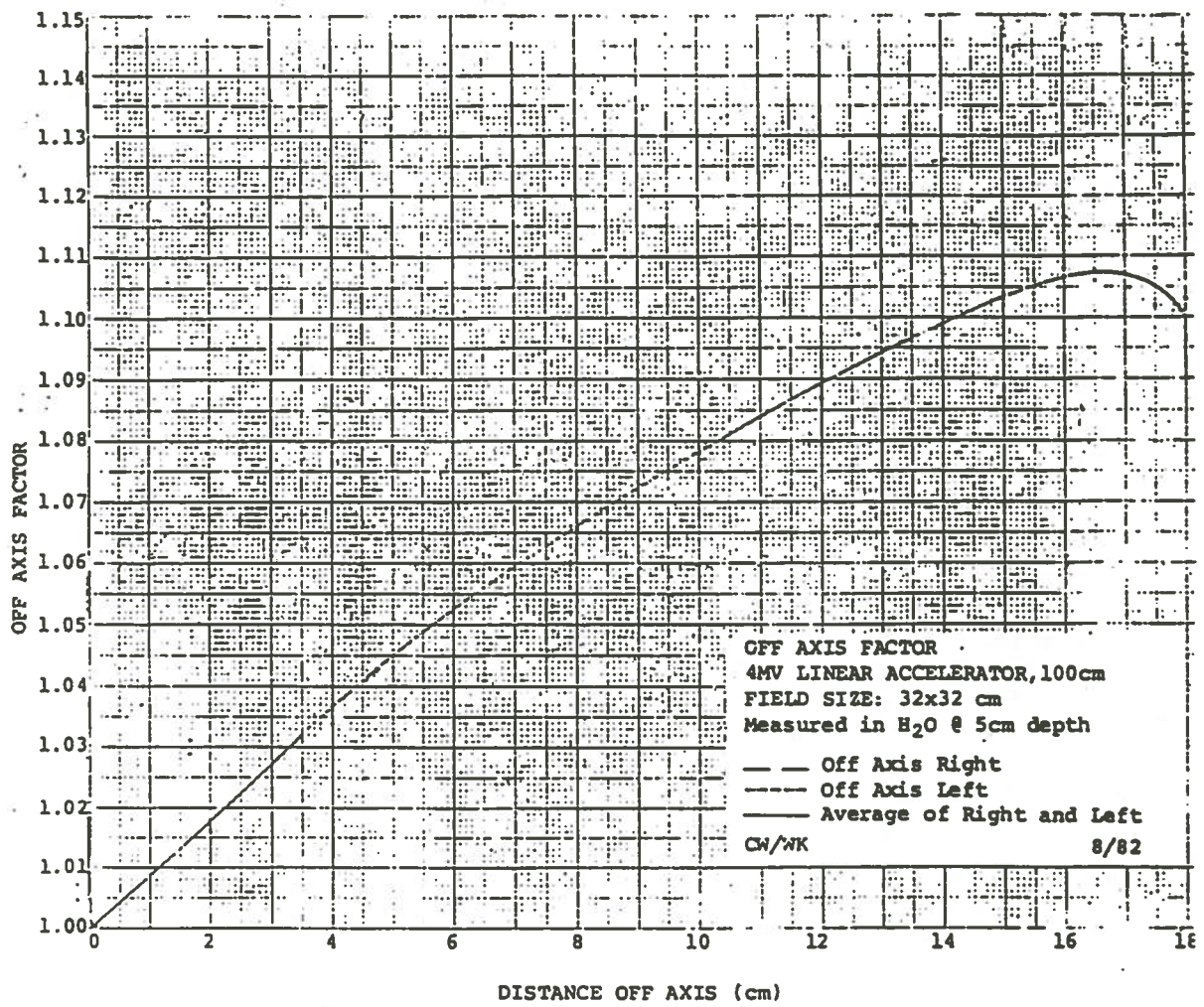

Figure B.2 Graph of the relationship between the off-axis factor and the distance in cm off the central axis, measured in water at a 5 cm depth (Kubricht, 1986).

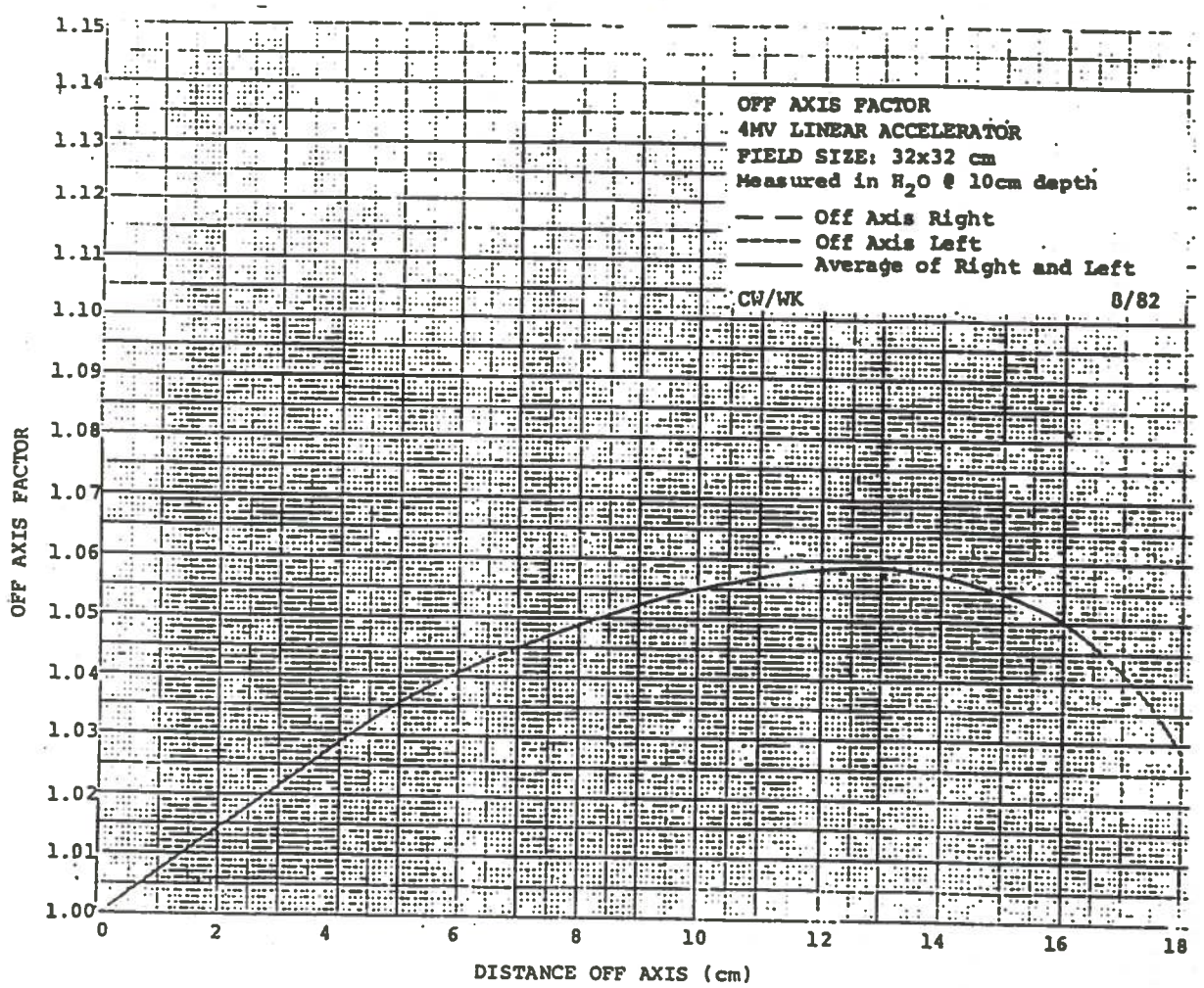

Figure B.3 Graph of the relationship between the off-axis factor and the distance in cm off the central axis. measured in water at a 10 cm depth (Kubricht, 1986).

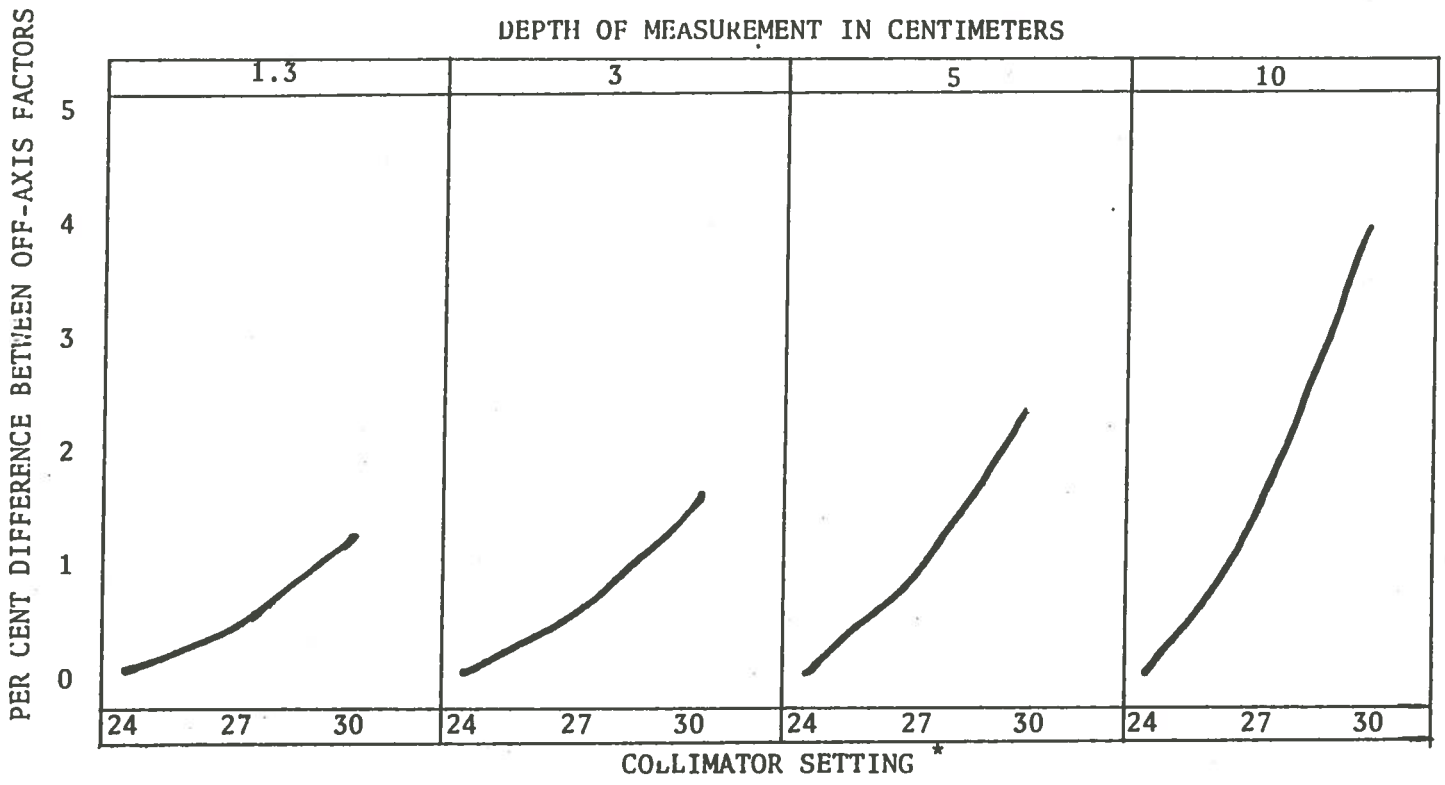

*The single number denotes the same diminsion in both the length and width directions

Figure B.4 Graphs showing the effect of increasing the field size on the off-axis factor for a point at a given distance from the central axis of the radiation beam.

APPENDIX C

CALCULATION OF SCATTER/AIR RATIO

The average scatter/air ratio for any point is calculated by summing the contributions from a number of sectors with equal angles as demonstrated in Figure C.1. The scatter/air ratio for various circular field sizes for a given depth are marked on a ruler for direct reading. A different ruler is prepared for each depth of calculation. Blocked portions of the field are considered to contribute no scatter and SAR values for these portions of the field are subtracted (Table C.1). The sum of the contributions of all of the sectors is divided by the number of sectors (Table C.1).

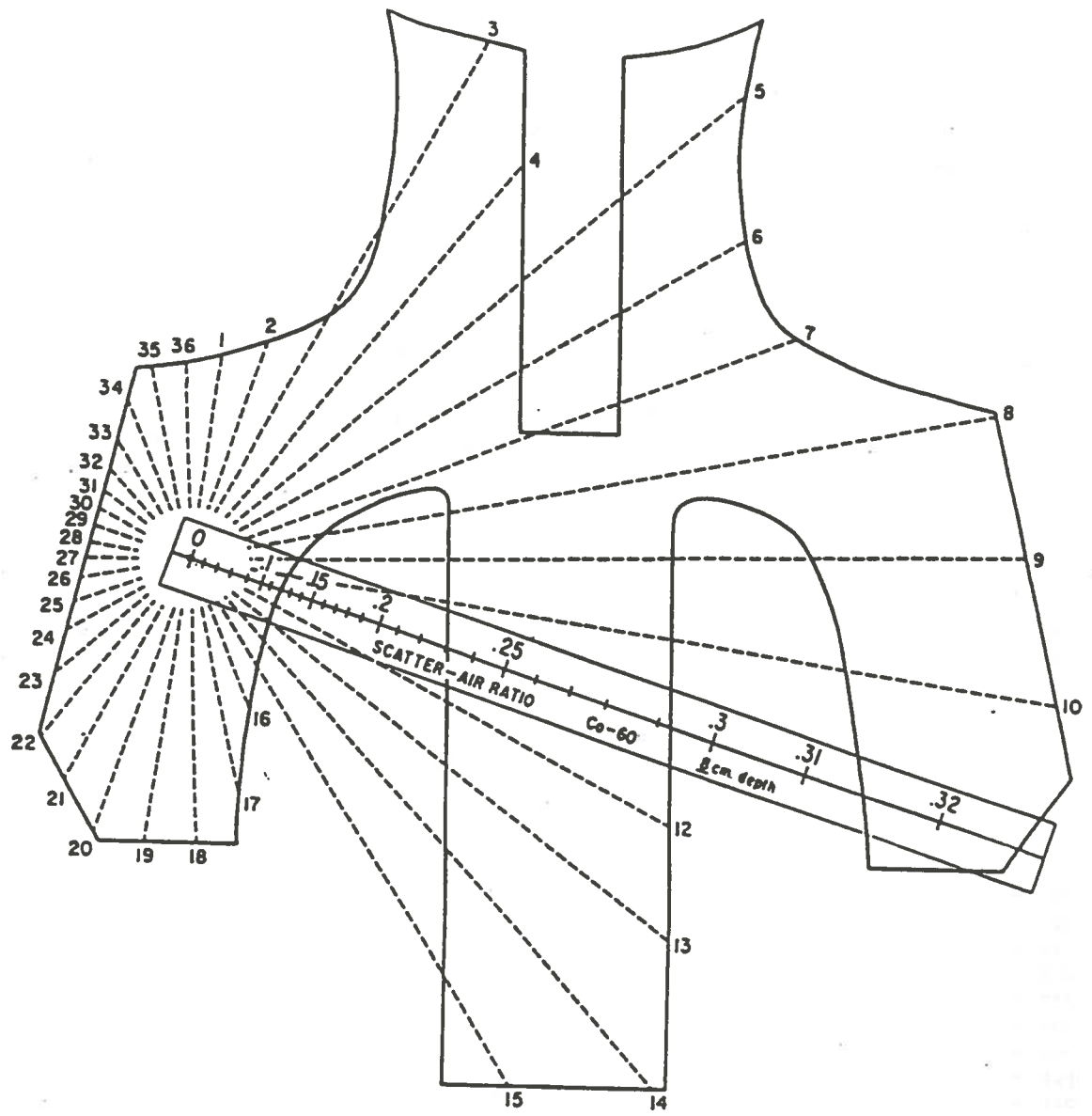

Figure C.1 An example of the method of obtaining the average scatter/air ratio from equal sectors centering on a point of interest. Taken from Cundiff, et al. (1973).

Table C.1 An example of the calculation of the average scatter/air ratio to the point in Figure C.1. Taken from Cundiff, et al. (1973).

Sector	Scatter/Air Ratio (SAR)					Net SAR
1	+.208					+.208
2	+.218					+.218
3	+.306	+.238	−.269			+.275
4	+.297					+.297
5	+.316	+.280	−.302			+.294
6	+.310	+.266	−.292			+.284
7	+.310	+.263	−.284			+.289
8	+.321	+.158	−.228			+.251
9	+.321	+.288	+.134	−.308	−.227	+.208
10	+.322	+.289	+.125	−.311	−.228	+.197
11	+.323	+.292	+.121	−.314	−.231	+.191
12	+.300	+.122	−.239			+.183
13	+.307	+.127	−.249			+.185
14	+.315	+.137	−.266			+.186
15	+.308	+.150	−.289			+.169
16	+.180					+.180
17	+.223					+.223
18	+.238					+.238
19	+.240					+.240
20	+.242					+.242
21	+.228					+.228
22	+.219					+.219
23	+.192					+.192
24	+.165					+.165
25	+.149					+.149
26	+.140					+.140
27	+.132					+.132
28	+.130					+.130
29	+.130					+.130
30	+.132					+.132
31	+.138					+.138
32	+.149					+.149
33	+.164					+.164
34	+.188					+.188
35	+.200	Average SAR $= \frac{7.216}{36} = .200$				+.200
36	+.202					+.202
					Total	+7.216

VITA

Tracie Davis Espenan was born July 30, 1958, in Natchez, Mississippi. She graduated from Huntington School, Inc., Ferriday, Louisiana in 1976. She received a Bachelor of Science degree in Science Education from Louisiana Tech University in May, 1979. In August, 1981, she received a Bachelor of Science degree in Medical Technology from Northeast Louisiana University. She entered graduate school in August, 1984 at Louisiana State University. She is currently a candidate for the Master of Science degree in Nuclear Science, Medical Radiation Science option.